

# Neuropathological Characteristics of Brachial Plexus Avulsion Injury With and Without Concomitant Spinal Cord Injury

Zarina S. Ali, MD, Victoria E. Johnson, MBChB, PhD, William Stewart, MBChB, PhD, Eric L. Zager, MD, Rui Xiao, PhD, Gregory G. Heuer, MD, PhD, Maura T. Weber, BA, Arka N. Mallela, MS, and Douglas H. Smith, MD

## Abstract

Neonatal brachial plexus avulsion injury (BPAI) commonly occurs as a consequence of birth trauma and can result in lifetime morbidity; however, little is known regarding the evolving neuropathological processes it induces. In particular, mechanical forces during BPAI can concomitantly damage the spinal cord and may contribute to outcome. Here, we describe the functional and neuropathological outcome following BPAI, with or without spinal cord injury, in a novel pediatric animal model. Twenty-eight-day-old piglets underwent unilateral C5–C7 BPAI with and without limited myelotomy. Following avulsion, all animals demonstrated right forelimb monoparesis. Injury extending into the spinal cord conferred greater motor deficit, including long tract signs. Consistent with clinical observations, avulsion with myelotomy resulted in more severe neuropathological changes with greater motor neuron death, progressive axonopathy, and persistent glial activation. These data demonstrate neuropathological features of BPAI associated with poor functional outcome. Interestingly, in contrast to adult small animal models of BPAI, a degree of motor neuron survival was observed, even following severe injury in this neonatal model. If this is also the case in human neonatal BPAI, repair may permit functional restoration. This model also provides a clinically relevant

platform for exploring the complex postavulsion neuropathological responses that may inform therapeutic strategies.

**Key Words:** Axonal pathology, Brachial plexus avulsion, Inflammation, Motor neuron loss, Neonatal, Spinal cord injury, Upper trunk injury.

## INTRODUCTION

Neonatal brachial plexus injury (BPI) from severe birth trauma results in paralysis and/or loss of sensation in the affected limb in approximately 0.4 to 2.6 per 1000 live births in the United States, with a cumulative incidence of 0.15% (1–4). Remarkably, most infants fully recover within 3 to 6 months, suggesting that some integrity of the nerve structure remains and allows damaged axons to recover or regenerate. However, for the remaining 18% to 50% of cases, the damage causes persistent functional impairment, most likely due to nerve root avulsion. These injuries are accompanied by a variety of physical and psychological challenges for affected children during development (4, 5).

Nerve root avulsion is the most severe BPI at any age (6), and spontaneous recovery is generally not possible due to complete disconnection of the nerve structure and accompanying axons from the spinal cord (7). In neonates with BPI, the most common injury affects the upper trunk (85%), including both the C5 and C6 roots, and, less frequently, the C7 root (8). This type of lesion represents both a CNS and PNS injury because spinal motor neurons undergo degeneration due to deafferentation while peripheral axons rapidly degenerate once they are disconnected from the cell body (9). This disconnection causes immediate and permanent paralysis of the targeted muscles along with sensory dysfunction in the corresponding dermatomes.

The mechanical process of avulsing the nerve root also commonly causes direct damage to the spinal cord. Indeed, signal changes in the spinal cord are found with MRI in up to 20% of adult patients after avulsion injury (10–13); these have been noted to include hemorrhage, scarring, edema, and posttraumatic syrinx (14, 15). Surprisingly, while there is some indication of spinal cord damage in neonates with nerve root avulsion (16), there has been little characterization of the

From the Department of Neurosurgery (ZAS, VEJ, WS, ELZ, MTW, ANM, DHS), Penn Center for Brain Injury and Repair (ZAS, VEJ, WS, MTW, ANM, DHS), Department of Biostatistics and Epidemiology (RX), Perelman School of Medicine, University of Pennsylvania, Philadelphia, Pennsylvania; Department of Neuropathology, Queen Elizabeth University Hospital, Glasgow, UK (WS); Division of Neurosurgery, The Children's Hospital of Philadelphia, Philadelphia, Pennsylvania (GGH).

Send correspondence to: Douglas H. Smith, MD, The Robert F. Groff Professor of Neurosurgery, Vice Chairman for Research and Education, Department of Neurosurgery, Director of Penn Center for Brain Injury and Repair, 105 Hayden Hall, 3320 Smith Walk, University of Pennsylvania, Philadelphia, PA19104. E-mail: smithdou@mail.med.upenn.edu

This study was supported by National Institutes of Health grants NS056202, NS038104, NS092389, The American Association of Neurological Surgeons David Kline Award (ZA), and The Neurosurgical Research and Education Foundation Fellowship Grant (ZA). NHS Research Scotland Career Research Fellowship (WS).

The authors have no duality or conflicts of interest to declare.

clinical and neuropathological consequences or whether this influences the extent of survival of motor neurons. In addition, while a variety of experimental models for adult brachial plexus avulsion injury have been developed in multiple species (9, 17–38), there are few pediatric models and none that utilize large animal species to enhance clinical relevance (35, 39–41).

Here, we investigated the behavioral and neuropathological changes associated with brachial plexus avulsion injury in a pediatric swine model. We also characterized these changes in the setting of severe avulsion injury associated with spinal cord injury to describe the range of CNS and PNS sequelae resulting from BPI in neonates.

## MATERIALS AND METHODS

### Animals and Surgical Procedures

All surgical procedures were approved by the University of Pennsylvania Institutional Animal Care and Use Committee. The University of Pennsylvania is an Association for Assessment and Accreditation of Laboratory Animal Care-accredited institution. Due to anticipated high mortality during surgery and recovery for neonatal and nonweaned piglets, we selected 28-day-old male Yorkshire piglets (8–10 kg; Archer Farms, Darlington, MD). Three groups of animals were evaluated; avulsion alone ( $n = 2$ ), avulsion with myelotomy ( $n = 3$ ), and naïve ( $n = 2$ ) for a total  $n = 7$ . Notably, the considerable effort necessary to perform the large animal model precluded having a large  $n$ /group. Nonetheless, in consultation with the biostatistician on the project, it was determined that the study was sufficiently powered as described in the “Results” section.

Prior to surgery, animals were fasted with free access to water for 12 hours. Anesthesia was induced via intramuscular injection of midazolam (0.5–0.6 mg/kg) and ketamine (10–15 mg/kg) followed by inhaled isoflurane (4%, 70% N<sub>2</sub>O and 30% O<sub>2</sub>) via snout mask. Endotracheal intubation was performed using a 4.5-mm endotracheal tube and maintenance of anesthesia achieved via inhaled isoflurane (2%, 70% N<sub>2</sub>O and 30% O<sub>2</sub>). Intravenous access was obtained via cannulation of the ear vein, and normal saline (40 cc/hour) was administered for hydration throughout the procedure. Glycopyrolate (0.01–0.02 mg/kg) was administered subcutaneously to reduce airway secretions and enrofloxacin (5 mg/kg) was administered as a perioperative antibiotic within 30 minutes of incision.

In a surgical operating room, the animals ( $n = 5$ ) were positioned prone and the dorsal neck prepped in a sterile fashion. Bupivacaine (1–2 mg/kg) was injected along the midline dorsal line of incision. A midline dorsal incision from the occiput to the upper thoracic level was made and the paravertebral muscles were dissected from the spinous processes to expose the spinal vertebrae. The C5, C6, and C7 posterior spinal elements were identified by counting discrete vertebrae in a caudal to cranial direction using the first thoracic vertebra as a landmark. A C5–C7 laminectomy was performed followed by a right paramedian durotomy to expose the dorsal and ventral rootlets of the C5–C7 spinal levels. These rootlets were then mechanically avulsed in a rostral to caudal direction at each

level using a fine micronerve hook under operating microscope magnification. Specifically, avulsion was performed in the form of a peripheral intradural rupture, as described (42); the injury occurring just distal to the surface of the cord, thereby leaving small stumps of variable sized rootlets approximately 1 mm in length, attached to the spinal cord.

In 3 of the animals with nerve root avulsion, we immediately afterward induced direct damage to the spinal cord ventral horn white matter to mimic the most severe nerve root avulsion in humans. A 1- to 2-mm ventrolateral myelotomy was created using a fine micronerve hook at the same 3 levels (Fig. 1). The nerve rootlets on the left side were left unaltered. Following avulsion, hemostasis was achieved and the site was copiously irrigated with normal saline solution. The dura, muscle, and skin layers were closed using a combination of absorbable sutures. Animals were extubated and recovered from anesthesia. Prophylactic analgesia was provided in the form of subcutaneously administered sustained-release buprenorphine (0.12 mg/kg) on postoperative day 0, as well as daily meloxicam (0.4–0.6 mg/kg) until postoperative day 3.

### Clinical Assessment

Postoperatively, animals were clinically assessed in an open field for right and left forelimb and hindlimb muscle bulk, tone, and motor function on a weekly basis. A scoring system was devised to quantify motor function, as modified from standard clinical motor assessment. For forelimb function, animals were scored as demonstrating 1) flaccid forelimb, nonweight bearing, 2) spontaneous movement of forelimb with some weakness, nonweight bearing, 3) spontaneous movement of forelimb with little weakness, weight bearing, or 4) normal forelimb motor function. Motor function for the hindlimbs was scored similarly as 1) severe weakness of hindlimbs, nonweight bearing, 2) spastic hindlimbs with some weakness, weight bearing but abnormal gait, 3) spastic hindlimbs with little to no weakness, weight bearing, or 4) normal hindlimb function.

### Animal Perfusion and Tissue Handling

Six weeks following surgery, the 5 animals with BPI and an additional 2 naïve animals were anesthetized with intramuscular injection of midazolam (0.5–0.6 mg/kg) and ketamine (10–15 mg/kg) and subsequent mask ventilation with 5% isoflurane, 70% nitrous oxide (N<sub>2</sub>O), and 30% O<sub>2</sub>.

Both the left and right biceps muscles were biopsied and dissected for postfixation in either 10% neutral buffered formalin (NBF) for 48 hours followed by processing to paraffin, or rapid freezing in liquid nitrogen-chilled isopentane for subsequent storage at –80 °C. Next, animals underwent thoracotomy and transcardial perfusion with a 0.9%-heparinized saline flush followed by 10 liters of 10% NBF. The cervical spinal vertebrae and associated soft tissues were harvested en bloc and postfixed in 10% NBF for 48 hours to minimize handling artifact. The spinal cord and associated roots were then dissected and re-immersed in 10% NBF for a further 7 days before being blocked in the axial plane midway between the rootlets for each spinal level. Tissue was processed to paraffin

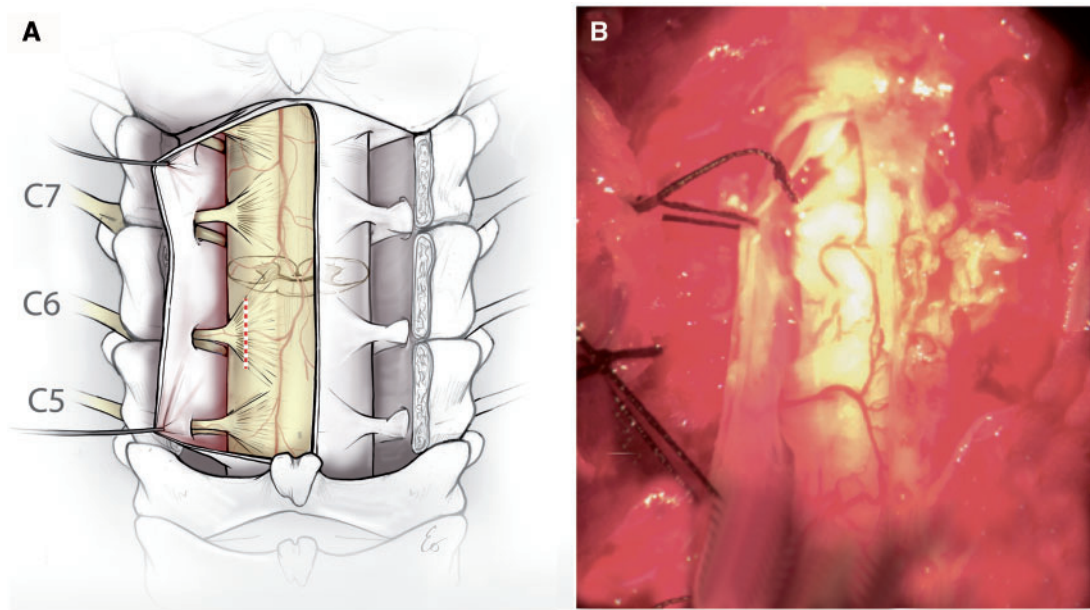


**FIGURE 1.** Experimental model of neonatal brachial plexus injury. **(A)** Schematic showing the axial section of the spinal cord C5–C7 from the surgeon’s point of view where the dorsal rootlets and dorsal horns are superficial and the ventral roots and ventral horns are deep. The red dotted line represents the site of avulsion. **(B)** Intraoperative photograph of the surgical approach.

using standard techniques using a Shandon Hypercenter XP tissue processor (Thermo Fisher Scientific, Waltham, MA), on a 62-hour cycle (43). Tissue was then embedded in paraffin wax. The relevant cord levels were sectioned in their entirety at a thickness of 10  $\mu\text{m}$ . Sets of serial sections at the desired intervals were then selected for staining as described below. For the BPI animals, C5–C7 were examined by all of the following techniques. For the naïve animals, only C5 and C6 were examined due to technical limitations.

### Hematoxylin and Eosin Staining

Standard hematoxylin and eosin (H&E) stains were performed on paraffin-embedded spinal cord sections 800  $\mu\text{m}$  apart. Slides were deparaffinized in xylene and rehydrated to water followed by immersion for 10 minutes in Mayer’s hematoxylin (Sigma, St Louis, MO). After rinsing and subsequent immersion in 1.5% aqueous lithium carbonate solution for 1 minute, slides were again rinsed and further immersed in 25% aqueous Shandon Eosin Y solution (Thermo Fisher Scientific, Waltham, MA) for 5 minutes. Differentiation was achieved using 95% ethanol followed by dehydration. Sections were cleared in xylenes and coverslipped with Cytoseal™ 60 (Thermo Fisher Scientific, Waltham, MA).

### Immunohistochemical Labeling

Paraffin-embedded sections were deparaffinized in xylene and rehydrated to water through a series of graded alcohols. Endogenous peroxidase activity was quenched by immersion in 3% aqueous hydrogen peroxide for 15 minutes. Antigen retrieval was then achieved by immersing slides in preboiled 0.1

M Tris EDTA (Sigma, St. Louis, MO) and heating within a pressurized microwave cooker for 8 minutes. Slides were blocked for 30 minutes in 1% normal horse or goat serum (Vector Laboratories, Burlingame, CA) in optimax buffer (Biogenex, Fremont, CA). Primary antibodies were then applied and allowed to incubate overnight at 4 °C. Goat anti-choline acetyltransferase (ChAT) (1:400; Millipore, Billerica, MA) was used to detect the presence of motor neurons; mouse anti- $\beta$ -amyloid precursor protein ( $\beta$ APP) (1:90 K, 22C11 clone; Millipore) was used to evaluate axonal degeneration (44–46); mouse anti-neurofilament (NF200) (1:3K; Sigma-Aldrich, St. Louis, MO) was used to detect axons; rabbit anti-calcitonin gene-related peptide (CGRP) (1:20K; Sigma-Aldrich) was used to detect sensory neurons; rabbit anti-Iba-1 (1:10K; Wako Chemicals Inc., Richmond, VA) was used to evaluate microglial activity; mouse anti-glial fibrillary acidic protein (GFAP) (1:40K; Millipore) was used to detect astrocytes; and Ab246 (1:9K; courtesy of Dr. Robert Siman, Univ. of Pennsylvania), specific for the caspase-derived fragment of  $\alpha$ -spectrin, was used to assess apoptosis (47–49). After rinsing in PBS, the appropriate biotinylated secondary antibodies were applied to all sections for 30 minutes. Specifically, for  $\beta$ APP, NF200, CGRP, Iba-1, and GFAP staining, slides received anti-mouse IgG/rabbit IgG from the Vectastain Universal Elite kit; Vector Laboratories) as per the manufacturer’s instructions (Vector Laboratories). For ChAT staining, slides received horse anti goat IgG at 1:200 (Vector Laboratories). All sections were then incubated with an ABC (avidin-biotin complex) for 30 minutes as per manufacturer’s instructions (Vector Laboratories) at room temperature. Visualization was achieved by applying the DAB (3, 3'-diaminobenzidine) peroxidase

substrate kit. The slides were counterstained with Mayer's hematoxylin and dehydrated in a series of graded alcohols (2 x 2 minutes in 95% ethanol followed by 2 x 2 minutes in 100% ethanol). Tissue was cleared in xylenes and coverslipped with Cytoseal 60.

### Luxol Fast Blue/Cresyl Violet

Following standard dewaxing and rehydration, paraffin-embedded spinal cord sections 400  $\mu\text{m}$  apart were immersed for 4 hours in Luxol fast blue (LFB) solution in 95% ethanol (Solvent Blue 38, Sigma, St Louis, MO) at 60 °C. Sections were differentiated using serial immersion in 2% aqueous lithium carbonate and 70% ethanol. After rinsing, sections were immersed in 0.1% aqueous Cresyl violet (CV) solution (Merck, Kenilworth, NJ) for 5 minutes at 60 °C. After rinsing, sections were differentiated, dehydrated in a series of graded alcohols as above, cleared in xylenes and coverslipped with Cytoseal 60.

### Adenosine Triphosphatase Staining of Skeletal Muscle Tissue

Adenosine triphosphatase (ATPase) staining at pH 9.4 was performed on cryostat sections of fresh frozen muscle tissue from both the right and left biceps using an established protocol (50). Briefly, 10- $\mu\text{m}$ -thick frozen sections from both the right and left biceps were sectioned on a cryostat and mounted on superfrost plus slides. Slides were agitated in a rinse solution (18 mM calcium chloride in 100 mM Tris buffer, pH 7.8) for 1 minute followed by preincubation in an alkaline solution (18 mM calcium chloride in 100 mM Sigma No. 221 alkaline buffer, pH 10.4; Sigma, St. Louis, MO) for 15 minutes at room temperature. After further rinsing in calcium chloride with agitation, slides were incubated in an alkaline solution containing 2.7 mM ATP (50 mM potassium chloride, 18 mM calcium chloride in 100 mM Sigma No. 221 alkaline buffer, pH 9.4) for 30 minutes at 37 °C. Slides were then rinsed in 1% calcium chloride (3 x 30 seconds), immersed in 2% cobalt chloride for 3 minutes, and washed in an alkaline solution (100 mM Sigma No. 221 alkaline buffer, pH 9.4) (4 x 30 seconds). Following immersion in 1% ammonium sulfide for 3 minutes, slides were rinsed in tap water, dehydrated in graded alcohols as above, cleared in xylenes, and coverslipped with Cytoseal 60.

### Nicotinamide Adenine Dinucleotide Hydrogen-Tetrazolium Reductase Staining of Skeletal Muscle Tissue

Nicotinamide adenine dinucleotide hydrogen-tetrazolium reductase (NADH-TR) staining was performed on cryostat sections of fresh frozen muscle tissue from both the right and left biceps using an established protocol (51). Briefly, 10- $\mu\text{m}$ -thick frozen sections were incubated for 30 minutes at 37 °C in NADH solution (1 mg of NADH per 1 mL of a stock solution containing 0.4 M nitroblue tetrazolium and 0.2 M Tris buffer [pH 7.4]). Following incubation, slides were rinsed in gently flowing deionized water and immersed

in 10% NBF for 10 minutes. After further rinsing, slides were coverslipped in an aqueous mounting medium (DAKO, Carpinteria, CA).

### Analyses of Histological Findings

Serial axial spinal cord sections were selected (400  $\mu\text{m}$  apart; approximately 8 sections per spinal cord level) and all ChAT-positive motor neurons were counted on both the intact and lesioned side of the C5, C6, and C7 spinal segments. Because ChAT immunoreactivity may be changed as a consequence of injury, serial sections stained with CV were also used to quantify the motor neurons as an independent marker. Only CV-positive cells with a visible nucleus were included.

The study power was enhanced due to the subsampling in each of the spinal segments. All cells with positive staining for ChAT or nucleated CV-positive cells in Rexed layer IX were analyzed and counted by 2 independent investigators blinded to all clinical details. Inter-rater reliability of observations was found to be consistent (intraclass correlation = 0.921). The mean number of motor neurons in individual spinal levels and across all 3 spinal levels (C5–C7) both ipsilateral and contralateral to the lesion was determined per animal. The mean number of surviving neurons between groups was compared using mixed-effect linear models. The comparisons we made included ipsilateral versus contralateral at the same spinal level for each of the 3 groups (avulsion only, avulsion with myelotomy, and naïve control), as well as pairwise comparison between the 3 groups at each spinal level. In the mixed-effect model, a subject (piglet)-specific random effect was included to account for potential correlation among sections of the spinal segment from the same animal, or a random effect included to account for pairing relationship between the ipsilateral and contralateral at the same spinal level of the same group.

The extents of axonal pathology and glial responses were evaluated using semiquantitative scoring systems. Notably, the direct quantification of axons is notoriously challenging, in particular swollen regions along an individual axon may travel in and out of plane in the same section or traverse multiple sections; in addition, axons may be fragmented. As such, standard approaches using percentage area and profile counting fail to provide meaningful quantification of individual axon numbers; therefore, a semiquantitative approach was warranted. Specifically, 10- $\mu\text{m}$  spinal cord cross sections every 800  $\mu\text{m}$  (approximately 4 sections per cord level) for levels C5, C6, and C7 stained for  $\beta\text{APP}$  were scored in 6 cord subregions both ipsilateral and contralateral to the lesion: dorsal root entry zone (DREZ), ventral root entry zone (VREZ), and the ventral horn. Semiquantitative analysis scores were assigned as follows. To assess axonal degeneration, the extent of swollen  $\beta\text{APP}$ -reactive profiles was classified as 0 = absent; 1 = minimal; 2 = moderate; or 3 = extensive.

To assess glial reactivity, serial sections (as above at 800  $\mu\text{m}$  apart) were examined for GFAP and Iba-1 immunoreactivity in the same regions. Blinded semiquantitative analyses were selected to encompass the complex morphological alterations over large tissue areas. Sections were examined

for classical microglial phenotypes consistent with increasing activation including hypertrophy of the cell body, and retraction and thickening of microglial ramifications. An increasing predominance of these morphologies was semiquantitatively classified as, 0 = no activation; 1 = minimal activation; 2 = moderate activation; 3 = extensive activation with frank amoeboid morphologies. To assess astrogliosis, sections were examined for classical phenotypes of reactive astrocytes including increased reactivity to GFAP, somatic hypertrophy, and an increased number and thickness of processes. An increasing predominance of these morphologies was semiquantitatively classified as follows: 0 = no activation; 1 = minimal activation; 2 = moderate activation; 3 = extensive activation.

An overall pathology score for each section was obtained by calculating the average of the 6 individual subregional scores per individual spinal level and across all 3 spinal levels both ipsilateral and contralateral to the lesion for each animal.

## RESULTS

### Functional Assessment

Animals underwent surgery without unintended morbidity or mortality. Immediately postoperatively, all animals demonstrated significant, acute, right forelimb dysfunction (Fig. 2A). All animals were nonweight bearing in the right forelimb and demonstrated flaccid monoparesis of that limb, which occurred immediately postoperatively and remained stable over 6 weeks (average score = 1). Muscle bulk in the right forelimb was noted to decrease over 6 weeks. Despite this, the animals were able to ambulate without significant disability, access food and water freely, and socially interact.

In addition to right forelimb weakness, the avulsion with myelotomy group also demonstrated some bilateral hindlimb weakness, which was notably worse on the right side.

This was evident immediately after surgery and remained stable over 6 weeks (average ipsilateral score = 3.3; average contralateral score = 2) (Fig. 2B). Animals in this group were able to maintain weight-bearing status in the hindlimbs but did demonstrate spasticity with ambulation. Muscle bulk was noted to be grossly unchanged in the hind limbs. These animals, while significantly more disabled, were able to access food and water and socially interact with animals housed in the same pen. No intraoperative or postoperative complications, including bleeding, hemorrhage, infection, or damage to surrounding anatomical structures occurred in any animals.

### Gross Pathological Findings

At 6 weeks following injury, deformity of the spinal cord at each segment was observed on the avulsed side, as demonstrated grossly and via histopathology performed on whole axial cord sections. Specifically, there was gross deformity of the hemicord ipsilateral to the mechanical avulsion injury when compared to the contralateral side. In particular, the ventral horn of the spinal cord was also noted to be deformed. At the site of avulsion, there was clear disruption of the white matter with complete disconnection of the rootlet.

### Motor Neuron Changes: ChAT-Positive Neurons

At 6 weeks following injury, animals were found to have fewer ChAT-positive neurons in the ipsilateral, avulsed side of cord when compared to the contralateral, uninjured, side in both animals with and without myelotomy. Specifically, this decrease in ChAT-positive neurons was also present at each individual spinal level in the avulsion plus myelotomy group C5 ( $p < 0.0001$ ), C6 ( $p < 0.0001$ ), C7 ( $p < 0.0001$ ), and all levels combined ( $p < 0.0001$ ). Similarly following avulsion only, decreased ChAT-positive neurons

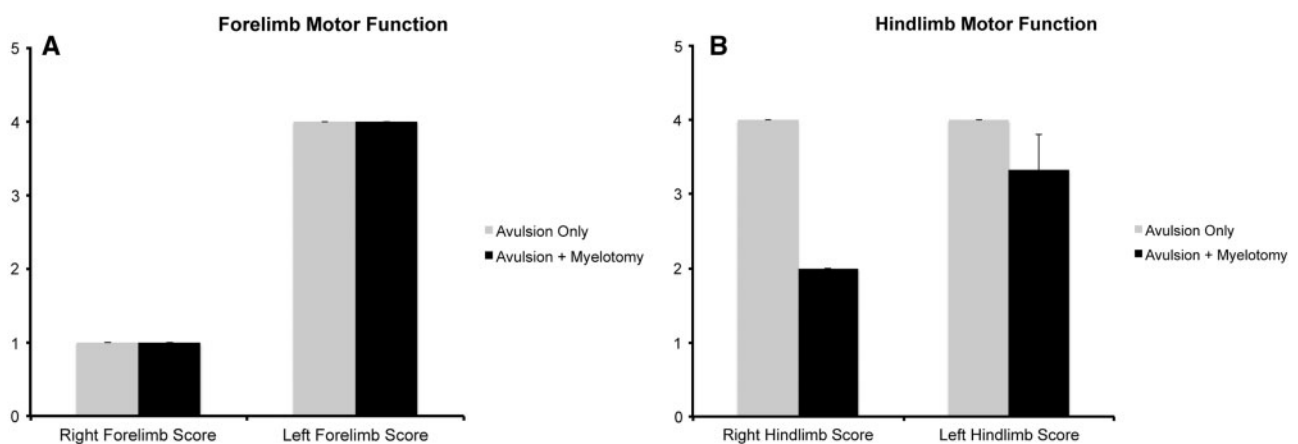


**FIGURE 2.** Forelimb (A) and hindlimb (B) function score at 6 weeks following avulsion with (n=3) or without (n=2) myelotomy. Forelimb motor function scoring: 1) = flaccid forelimb, nonweight bearing, 2 = spontaneous movement of forelimb with some weakness, nonweight bearing, 3 = spontaneous movement of forelimb with little weakness, weight bearing, or 4 = normal forelimb motor function. Hindlimb motor function scoring: 1 = severe weakness of hindlimbs, nonweight bearing, 2 = spastic hindlimbs with some weakness, weight bearing but abnormal gait, 3 = spastic hindlimbs with little to no weakness, weight bearing, or 4 = normal hindlimb function.

were also present at each individual spinal level C5 ( $p < 0.0001$ ), C6 ( $p = 0.002$ ), C7 ( $p < 0.0001$ ), and all levels combined ( $p < 0.0001$ ) (Figs. 3A, C, E, 4A–D).

In addition, there was a clear injury effect when compared to naïve animals. Specifically, following avulsion with myelotomy, there were decreased ChAT-positive neurons on the ipsilateral side when compared to naïve animals at each spinal level, C5 ( $p < 0.0001$ ), C6 ( $p < 0.0001$ ), and all levels combined ( $p < 0.0001$ ). However, there was no statistical difference when the contralateral side was compared to naïve C5 ( $p = 0.83$ ), C6 ( $p = 0.37$ ), and all levels combined ( $p = 0.46$ ). Following avulsion only, there were decreased ChAT-positive neurons on the ipsilateral side when compared to naïves at spinal level C6 ( $p < 0.0001$ ), and all levels combined ( $p < 0.0001$ ). In contrast, however, this did not reach significance at the C5 level ( $p = 0.094$ ), suggesting some sparing of motor neuron loss. Notably, there was no statistical difference in ChAT-positive neurons when the contralateral side was compared to naïve control C5 ( $p = 0.16$ ), C6 ( $p = 0.55$ ), and all levels combined ( $p = 0.36$ ).

Animals that underwent avulsion with myelotomy demonstrated more severe ventral horn damage than animals undergoing avulsion only. Specifically, following avulsion with myelotomy, there were decreased ChAT-positive neurons when compared to the avulsion-only group when comparing all spinal levels combined ( $p = 0.038$ ). Interestingly, this difference was not uniform across all levels. Specifically, there was a decreased number of ChAT-positive neurons in avulsion with myelotomy group versus avulsion only in the C6 level ( $p < 0.001$ ), with no significant difference at the C5 ( $p = 0.12$ ) and C7 levels ( $p = 0.14$ ).

No differences were detected in numbers of ChAT-positive neurons in the contralateral side between the avulsion with myelotomy versus avulsion only at C5 ( $p = 0.58$ ), C6 ( $p = 0.13$ ), C7 ( $p = 0.62$ ), and all levels combined ( $p = 0.30$ ) (Fig. 3A, C, E).

### Motor Neuron Changes: Quantification of CV-Stained Cells

Because ChAT immunoreactivity may change with injury independent of cell loss, the analysis was repeated using CV as a marker of all neurons in the ventral horn (Fig. 3B, D, F). Consistent with findings using ChAT immunohistochemistry (IHC), animals were found to have fewer neurons in the ipsilateral, avulsed side of cord when compared to the contralateral, uninjured, side in both animals with and without myelotomy. Specifically, this decrease in CV-positive neurons was also present at each individual spinal level in the avulsion plus myelotomy group C5:  $p < 0.0001$ ; C6:  $p < 0.0001$ ; C7:  $p < 0.0001$ ; and all levels combined:  $p < 0.0001$ . Similarly, following avulsion only, decreased CV-positive neurons were also present at each individual spinal level C5:  $p = 0.025$ ; C6:  $p = 0.002$ ; C7:  $p < 0.0048$ ; and all levels combined:  $p < 0.0001$ .

Also consistent, there was a clear injury effect when compared to naïve animals. Specifically, following avulsion with myelotomy, there were decreased CV-positive neurons on the ipsilateral side when compared to naïves at each spinal

level (C5,  $p < 0.0001$ ; C6,  $p < 0.0001$ ; and all levels combined,  $p < 0.0001$ ). Interestingly, whereas there was no statistical difference when the contralateral side was compared to controls at the C5 level ( $p = 0.63$ ) and all levels combined ( $p = 0.19$ ), there was a significant difference at the C6 level ( $p = 0.068$ ), indicating a possible contralateral effect.

Following avulsion only, there were decreased CV-positive neurons on the ipsilateral side when compared to naïves at spinal level C6 ( $p = 0.0056$ ) and all levels combined ( $p < 0.0001$ ); however, this did not reach significance at the C5 level ( $p = 0.54$ ), suggesting some sparing of motor neuron loss consistent with the ChAT findings. Notably, there was no statistical difference in CV-positive neurons when the contralateral side was compared to naïve controls (C5,  $p = 0.96$ ; C6,  $p = 0.20$ ; and all levels combined,  $p = 0.23$ ).

Animals that underwent avulsion with myelotomy demonstrated more severe ventral horn damage than animals undergoing avulsion only. Specifically, following avulsion with myelotomy, there were decreased ipsilateral CV-positive neurons when compared to the avulsion-only group when comparing all spinal levels combined ( $p < 0.001$ ). This difference was significant across all levels (C5,  $p < 0.0001$ ; C6,  $p < 0.0049$ ; C7,  $p < 0.007$ ).

Intriguingly, where counting of ChAT-positive neurons revealed no differences in the contralateral side between the avulsion with myelotomy versus avulsion only, counting using CV-positive cells indicates some contralateral effect at the C6 level ( $p = 0.0024$ ), and all levels combined ( $p = 0.0004$ ); however, no differences were observed at C5 ( $p = 0.54$ ) or C7 ( $p = 0.50$ ).

In all animals that underwent myelotomy, there was no evidence of direct mechanically induced injury to the spinal cord gray matter (via the micronerve hook) that could potentially contribute to motor neuron injury and loss. Notably, the remaining neurons appeared morphologically intact in both groups and only 2 animals from the avulsion with myelotomy group displayed occasional ( $< 10$ ) neurons positive for the caspase-derived fragment of  $\alpha$ -spectrin, which is indicative of ongoing cell death (47–49) (Fig. 4E, F). Interestingly, consistent with previous observations (52, 53), CGRP immunoreactivity could be observed in ventral horn neurons following both avulsion only and avulsion with myelotomy.

### White Matter Injury

At the site of avulsion, there was complete disconnection of the rootlet with an absence of NF-200-positive axons travelling from the rootlet into cord. In addition, LFB staining of the white matter tracts in the spinal cord ipsilateral to avulsion revealed a loss of white matter integrity. Specifically, at the DREZ and VREZ, there was a reduction in the overall density of staining for myelin (LFB), but also structural and organizational disruption of the spinal cord white matter (Fig. 5A, B). White matter degeneration was most pronounced in the animals that underwent avulsion with myelotomy, which also demonstrated foci of marked white matter degeneration in the ventrolateral spinal cord in

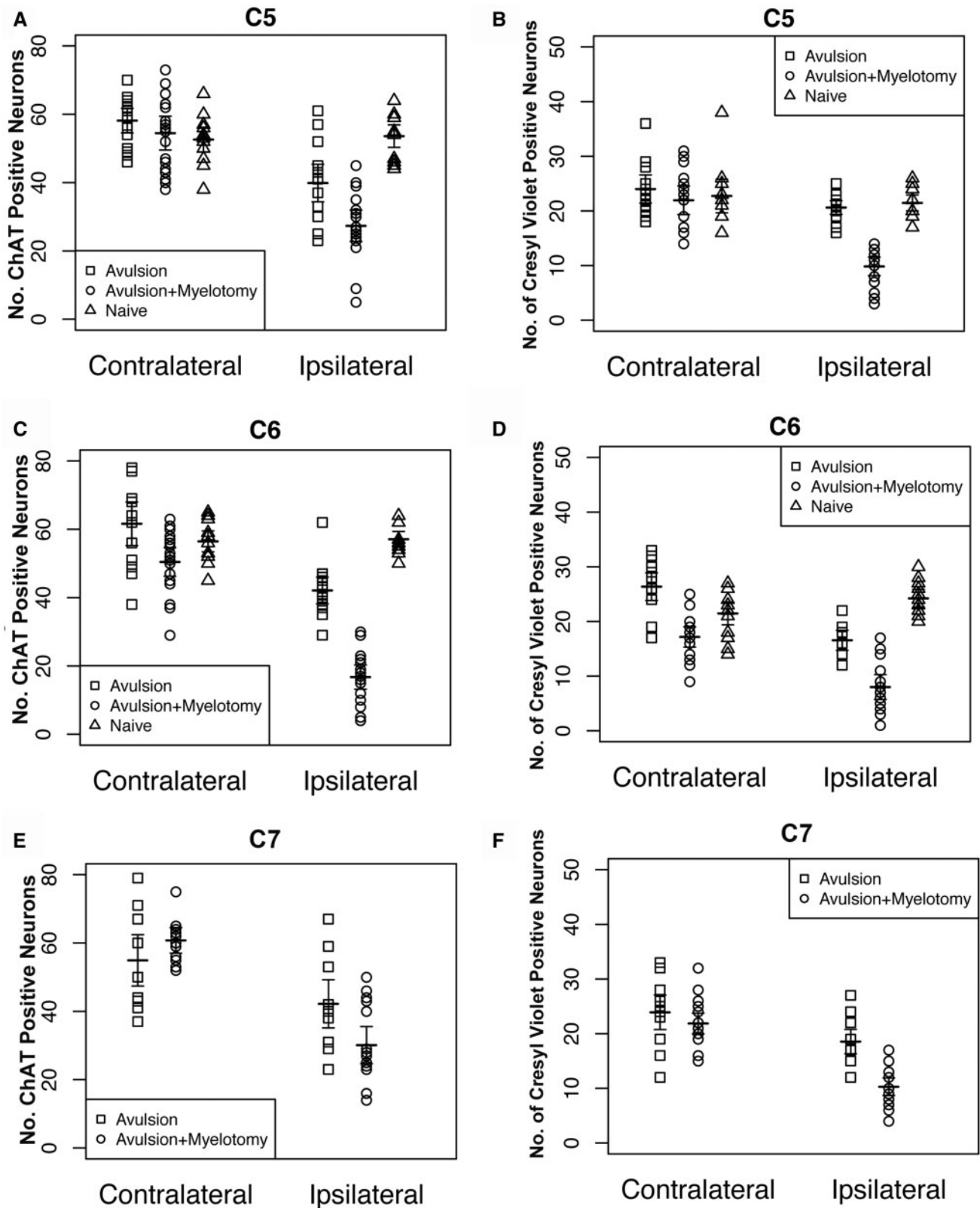


**FIGURE 3.** Graphs showing motor neuron counts for spinal levels C5–C7 for all individual animals as quantified using both anti-choline acetyl transferase (ChAT) immunohistochemistry (**A, C, E**) and Cresyl violet staining (**B, D, F**). Note the horizontal lines indicating the mean value for groups.

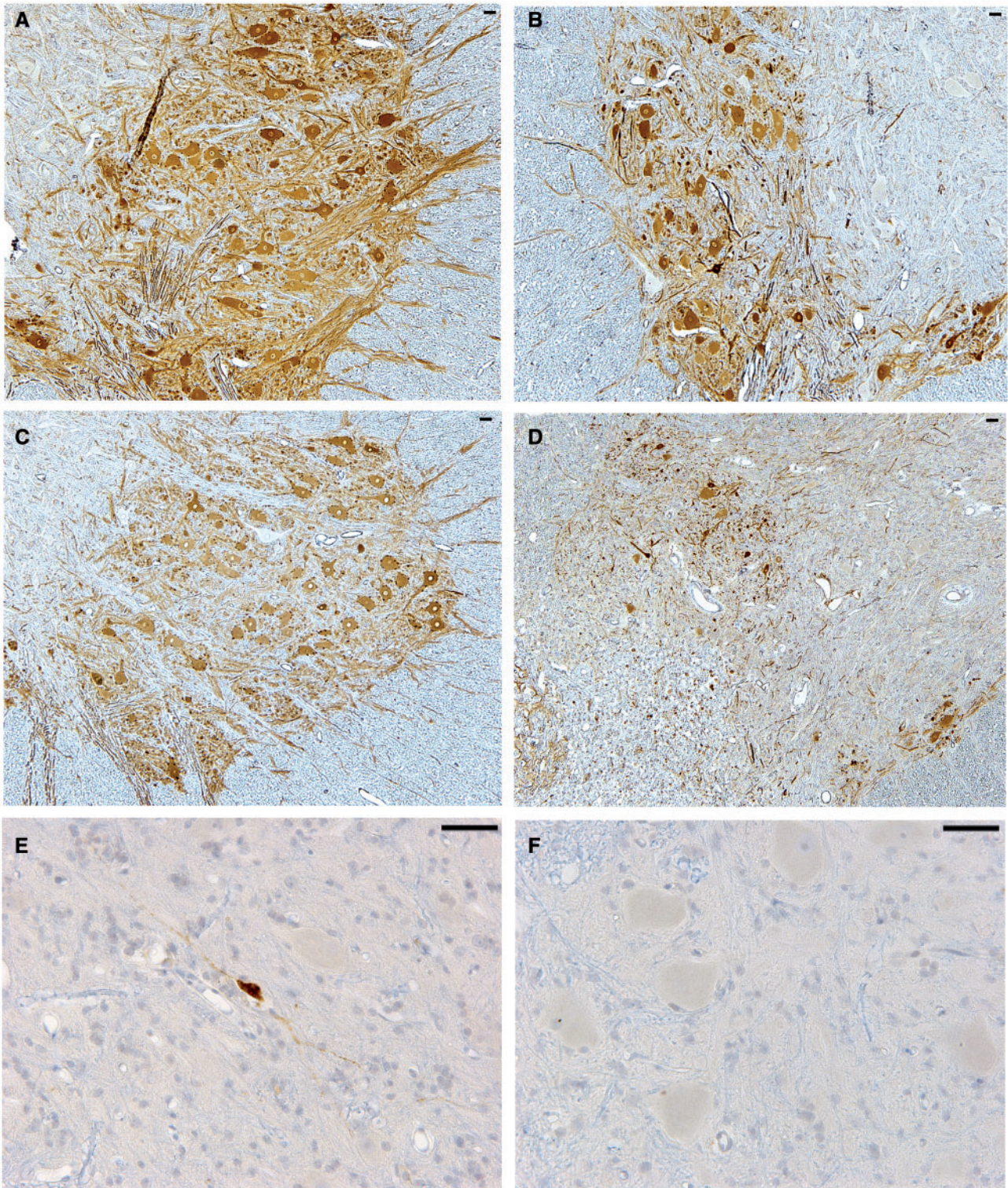


**FIGURE 4.** Representative images of choline acetyl transferase (ChAT) immunohistochemistry (IHC) showing surviving motor neurons in the contralateral (**A**) and ipsilateral (**B**) ventral horn at the C6 spinal cord level 6 weeks following avulsion only. This compares to ChAT IHC in the contralateral (**C**) and ipsilateral (**D**) ventral horn 6 weeks following avulsion with myelotomy. Notably, only very occasional ipsilateral surviving neurons were positive for the apoptotic marker Ab246, which detects a caspase-derived fragment of alpha-spectrin as shown in (**E**) at the C6 level. Indeed, the vast majority of cells were not immunoreactive for this marker (**F**) and appeared morphologically intact, indicating an absence of ongoing cellular degeneration. All scale bars = 50  $\mu$ m.

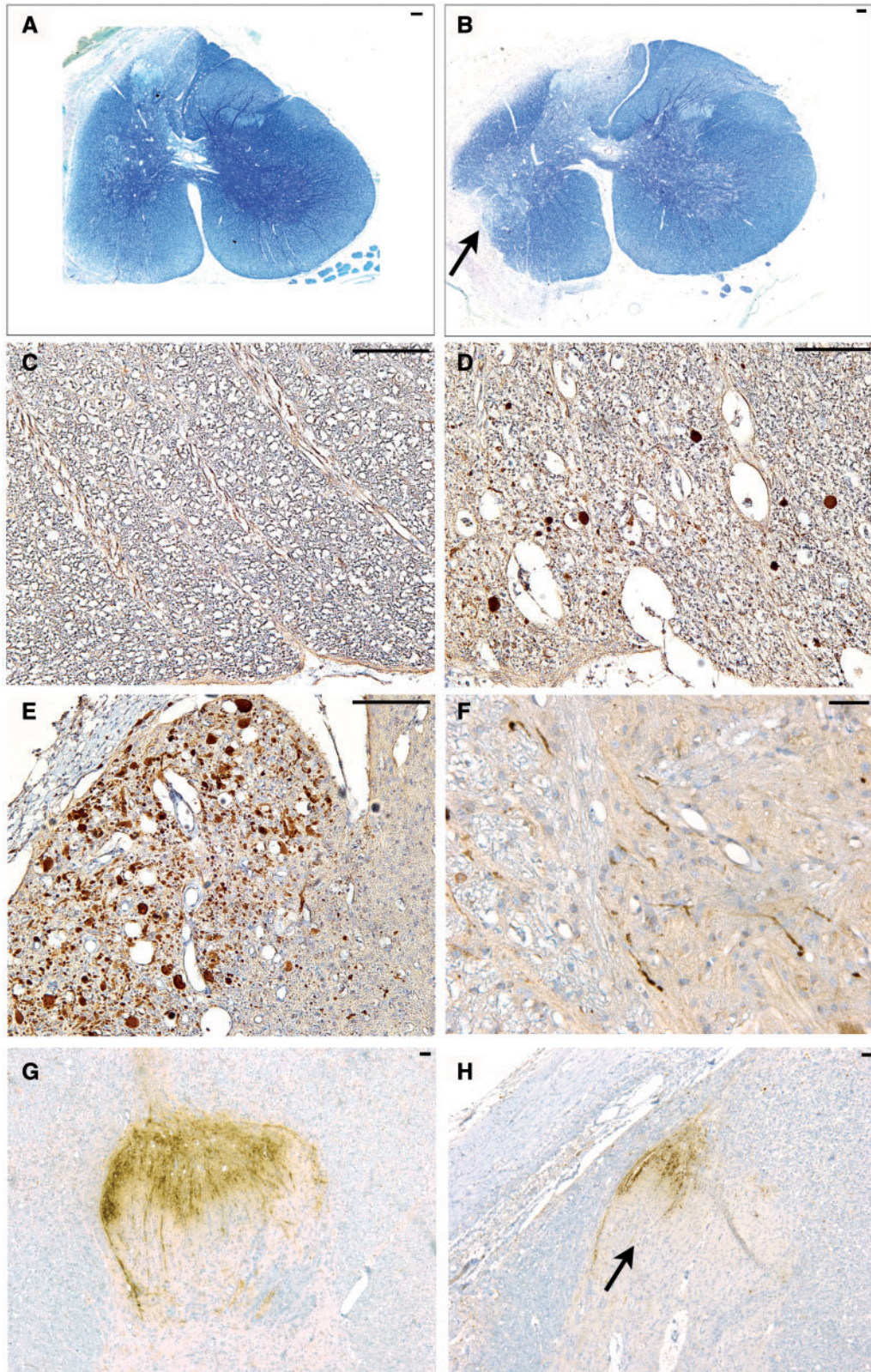


**FIGURE 5.** Representative images of white matter injury and ongoing axonal degeneration at 6 weeks postinjury. **(A)** Whole Luxol fast blue (LFB)/Cresyl violet (CV)-stained cross-sectional C5 spinal cord following avulsion only. Note the pallor in myelin staining corresponding to the dorsal root entry zone (DREZ) and ventral root entry zone (VREZ) ipsilateral to avulsion with

the region of the myelotomy (Fig. 5B). In contrast, animals that underwent avulsion only did not display any gross or microscopic evidence of direct mechanical injury to the spinal cord.

### Ongoing Axonal Degeneration

Ongoing axonal pathology was identified using IHC to visualize  $\beta$ APP as a marker of transport interruption;  $\beta$ APP can be observed accumulating within axonal bulbs or swollen and tortuous varicosities along the length of damaged axons (44, 46, 54). Clusters of granular axonal bulbs and varicosities were observed throughout the DREZ, the VREZ, and the ventral horn at 6 weeks following avulsion alone or avulsion with myelotomy (Fig. 5D–F). Although pathological alterations were primarily confined to the side of cord ipsilateral to the injury in all animals, rarely swollen axonal profiles were observed throughout the white matter of the cord contralateral to the lesion. Semiquantitative scoring revealed a greater extent and more widespread axonal pathology in the avulsion with myelotomy group versus the avulsion-only group (Fig. 8A). Notably, axonal bulbs in the ipsilateral DREZ and VREZ were more frequent with avulsion with myelotomy when compared to avulsion only (Fig. 5C–F). Naïve animals did not display any axonal pathology.

In addition, all injured animals demonstrated a loss of CGRP staining at the DREZ, indicating a loss of the central axonal processes of sensory neurons (Fig. 5G, H); however, this was not directly quantified. In addition, given that the dorsal root ganglia are outside of the spinal cord, we did not examine potential changes in dorsal horn axons.

### Glial Responses

Animals undergoing root avulsion with or without myelotomy also demonstrated microglial and astrocytic activity in the associated spinal cord segment. Specifically, there was greater microglial and astrocytic activation in sections stained for Iba-1 and GFAP in the ipsilateral hemicord compared to the contralateral hemicord in all animals (Figs. 6, 7). Reactive microglia displayed classic morphological appearances, including hypertrophy of the cell body, thickening and shortening of processes, and in some cases a frank amoeboid morphology consistent with a macrophage phenotype (Fig. 6). Reactive astrocytes displayed increased immunoreactivity to GFAP, somatic hypertrophy, and thickened cell processes (Fig. 7). A high density of glial cells with activated morphologies was

observed in clusters associated regionally with a high degree of axonal pathology. Regions of astrogliosis and microgliosis coincided. As determined using semiquantitative scoring, the degree of both microglial and astrocytic reactivity was greater in the avulsion with myelotomy group compared to the avulsion-only group (Fig. 8B, C). Specifically, the DREZ and VREZ regions ipsilateral to avulsion with myelotomy displayed a greater extent and more widespread distribution of reactive glial cells. Though the grey matter generally showed less microglial reactivity at the 6-week time point, there was a trend towards increased glial activity in the ipsilateral ventral horn in the avulsion with myelotomy group. Similarly, the avulsion with myelotomy group trended towards an increased glial response in the contralateral spinal cord. Naïve animals did not display any abnormal glial reactivity (Figs. 6I, J, 7I, J).

### Skeletal Muscle Atrophy

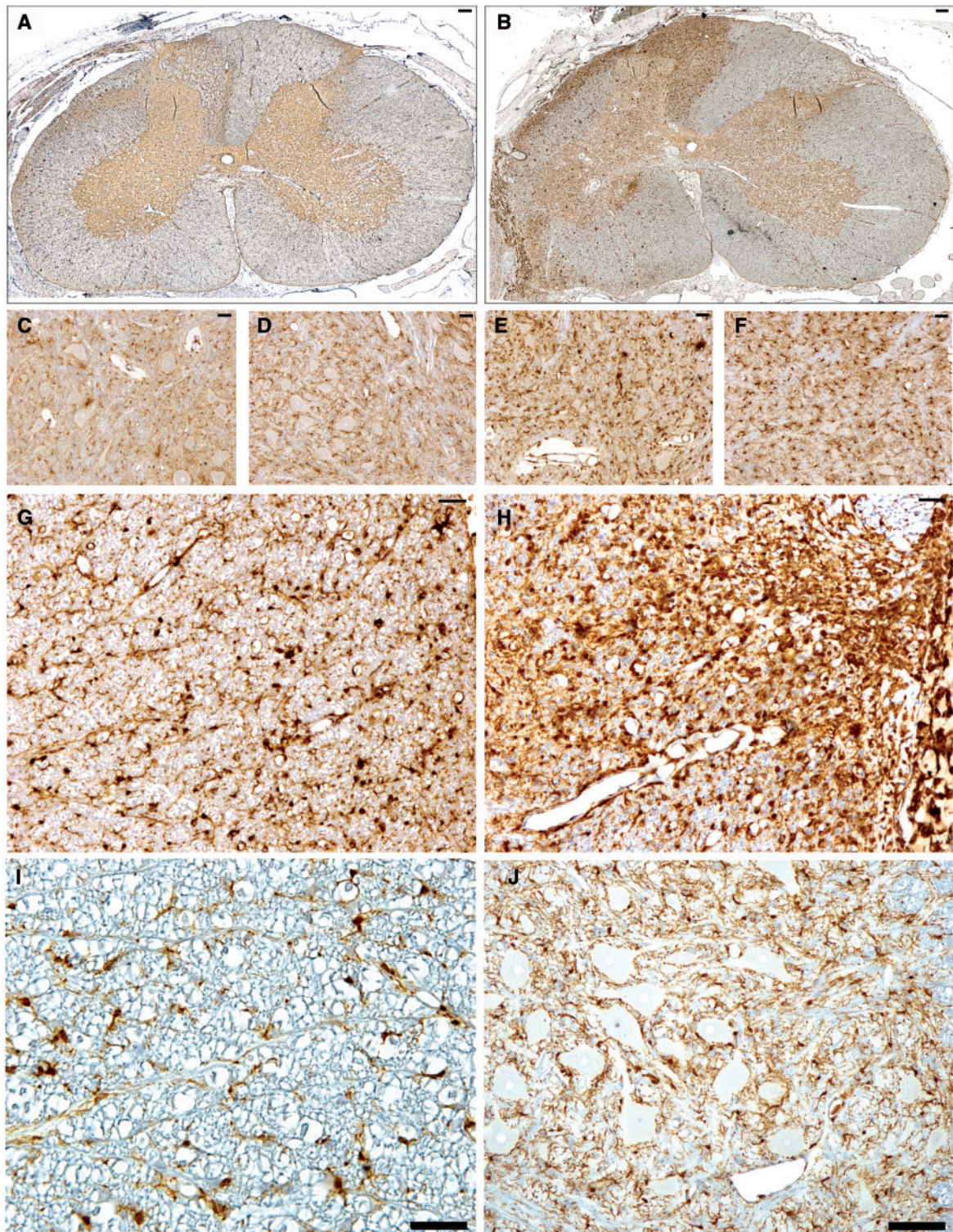
Examination of the right biceps muscle revealed profound atrophy at 6 weeks post-avulsion as identified on inspection and via palpation. This compared to the nonavulsed side (left) where there were no overt signs of atrophy. Histopathological examination confirmed the presence of profoundly atrophic biceps muscles on the side ipsilateral to the lesion when compared to the normal appearance of the contralateral biceps (Fig. 9). Specifically, the right biceps displayed fibers that were of small diameter and, frequently, angulated in profile. NADH-TR staining revealed numerous fibers with zones of central pallor surrounded by an outer zone of relatively darker staining typical of targetoid fibers, with clear peripheral accentuation of staining, and ATPase staining (pH 9.4) revealed fiber type grouping. Interestingly, fiber-typing studies indicated a degree of preferential type II fiber atrophy, in contrast to the reported mixed fiber atrophy typical of neurogenic atrophy in humans. As expected, no overt difference in the extent of neurogenic atrophy was observed between the avulsion only versus avulsion with myelotomy group.

### DISCUSSION

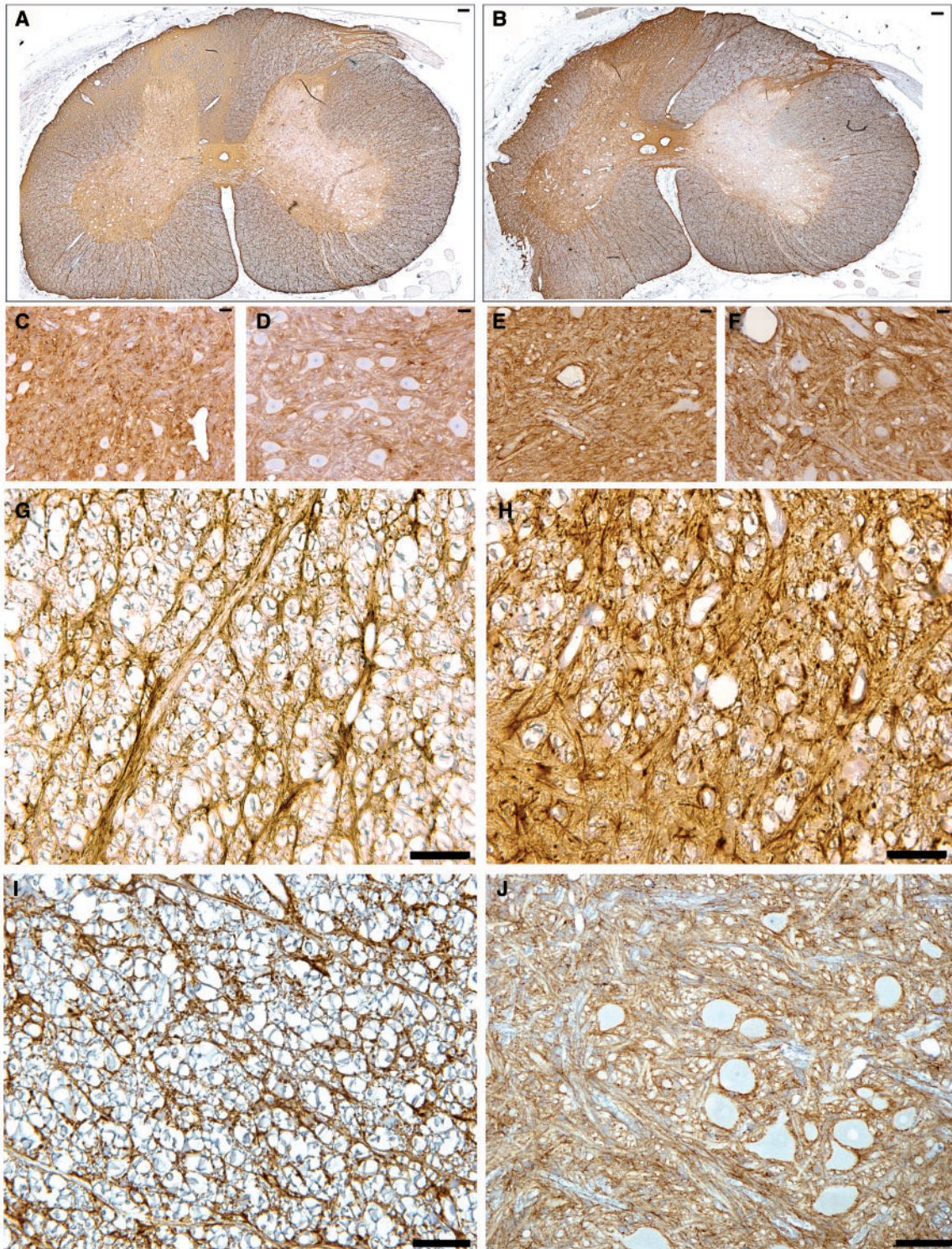
Using a clinically relevant model of brachial plexus injury in swine, we observed strikingly different functional outcomes and histopathology between animals that received severe avulsion injury alone compared to those with concomitant spinal cord injury. In particular, avulsion injury

FIGURE 5. Continued.

relative preservation of contralateral white matter integrity. (B) LFB/CV-stained cross-sectional C6 spinal cord following avulsion with myelotomy displaying marked pallor in myelin staining corresponding to extensive loss of white matter integrity in the DREZ and VREZ with relative preservation of contralateral white matter integrity. The arrow denotes the point of myelotomy. (C) An absence of amyloid precursor protein ( $\beta$ APP)-positive axonal pathology in the C6 contralateral VREZ following avulsion with myelotomy. (D) C6 ipsilateral DREZ displaying swollen APP-positive profiles indicating ongoing axonal pathology following avulsion with myelotomy. (E) Extensive axonal pathology ( $\beta$ APP-reactive) in the C7 VREZ ipsilateral to avulsion with myelotomy. (F) Swollen and varicose  $\beta$ APP-reactive axons in the gray-white interface of the C5 ventral horn ipsilateral to avulsion with myelotomy. (G, H) Abundant calcitonin gene-related peptide (CGRP) immunoreactivity in sensory processes were observed on the contralateral side of the C6 level (G). This compared to CGRP immunoreactivity showing more marked ipsilateral loss of sensory processes in the C6 spinal cord level following avulsion with myelotomy (H). Scale bars: A, B, 100  $\mu$ m; C–H, 50  $\mu$ m.



**FIGURE 6.** Whole spinal cord cross-section anti-Iba-1 stained sections demonstrate increased ipsilateral hemicord microglial activation following **(A)** avulsion only (C7) compared to the more extensive and widespread activation following **(B)** avulsion with myelotomy (C6). **(C-F)** High-magnification images display increased microglial clustering and reactivity in the C6 ipsilateral ventral horn following avulsion only **(C)**, C6 contralateral ventral horn following avulsion only **(D)**, C6 ipsilateral ventral horn following avulsion with myelotomy **(E)**, and C6 contralateral ventral horn following avulsion with myelotomy **(F)**. **(G-J)** Iba-1 immunoreactivity in C6 ipsilateral ventral root entry zone (VREZ) following avulsion only **(G)**, C6 ipsilateral VREZ following avulsion with myelotomy **(H)**, VREZ of naive animal showing minimal Iba-1 immunoreactivity **(I)**, and minimal Iba-1 immunoreactivity in the ventral horn of a naive animal **(J)**. Scale bars: **A, B, J**, 100  $\mu$ m; **C-I**, 50  $\mu$ m.



**FIGURE 7.** Whole spinal cord cross-sectional anti-glial fibrillary acidic protein (GFAP) immunostained sections demonstrate increased ipsilateral hemicord astrocytic activation following C7 avulsion only (**A**) compared to the more extensive and widespread activation following C6 avulsion with myelotomy (**B**). (**C–F**) High-magnification images display increased reactivity in the C7 ipsilateral ventral horn following avulsion only (**C**), C7 contralateral ventral horn following avulsion only (**D**), C6 ipsilateral ventral horn following avulsion with myelotomy (**E**), and C6 contralateral ventral horn following avulsion with myelotomy (**F**). (**G–J**) C6 ipsilateral ventral root entry zone (VREZ) following avulsion only (**G**), C6 ipsilateral VREZ following avulsion with myelotomy (**H**), VREZ of naïve animal showing minimal GFAP immunoreactivity (**I**), and minimal GFAP immunoreactivity in the ventral horn of a naïve animal (**J**). Scale bars: **A, B, J**, 100  $\mu$ m; **C–I**, 50  $\mu$ m.

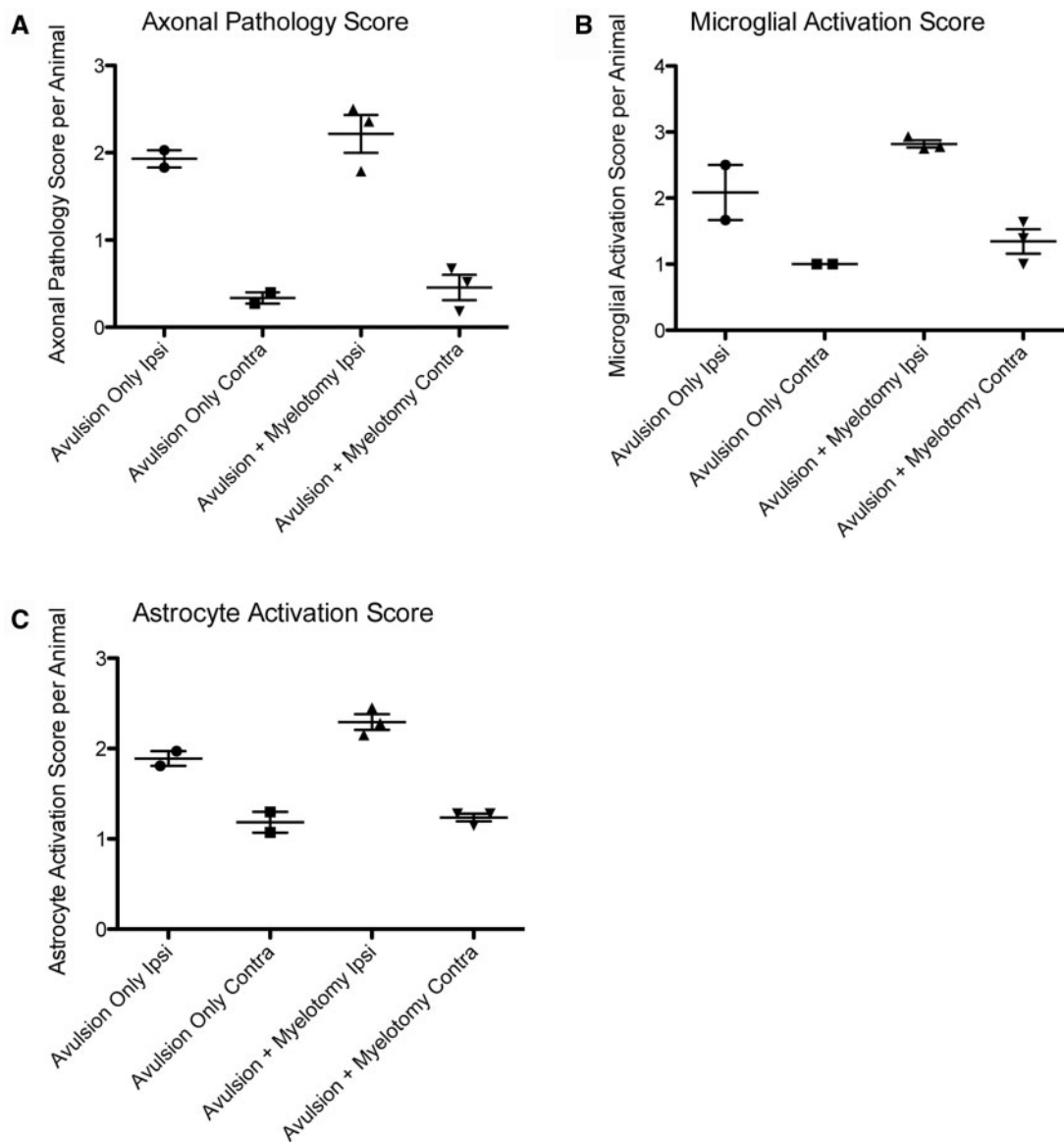


**FIGURE 8.** Graphs showing semiquantitative scores across groups for axonal pathology (A), microglial activation (B), and astrocytic activation (C), in the ipsilateral versus contralateral spinal cord following both avulsion only (n = 2) and avulsion with myelotomy (n = 3).

with associated myelotomy induced flaccid monoparesis of the forelimb in conjunction with long tract signs, which appear similar to the clinical manifestations of human brachial plexus injury. At the microscopic level, this motor dysfunction was accompanied by a more dramatic loss of spinal motor neurons in the ventral horn when compared to those with avulsion without injury to the spinal cord. Moreover, avulsion with myelotomy resulted in more pronounced and evolving white matter degeneration, with more extensive and persistent associated inflammatory and astroglial changes. Collectively, these data may have important clinical implications, demonstrating that the extent of white matter damage in association with nerve root avulsion plays a critical role in functional outcome. As such, these findings may inform

strategies to direct therapy for persisting changes postavulsion, including those targeted to chronic inflammation.

The poorer clinical outcome and more pronounced loss of spinal motor neurons in the nerve root avulsion plus myelotomy group compared with the avulsion-only group may be due to direct mechanical injury to the ventrolateral spinal cord. It has previously been shown in vivo that the more proximal axotomy is to the cell body, the more likely it will induce neuronal degeneration (55). This may also be true in nerve root avulsion with myelotomy, which presumably induces far more proximal disconnection of axons extending from the motor neurons. Notably, however, motor neuron loss was not complete even with this severe damage. In these animals, rescue or maintenance of ipsilateral motor neurons

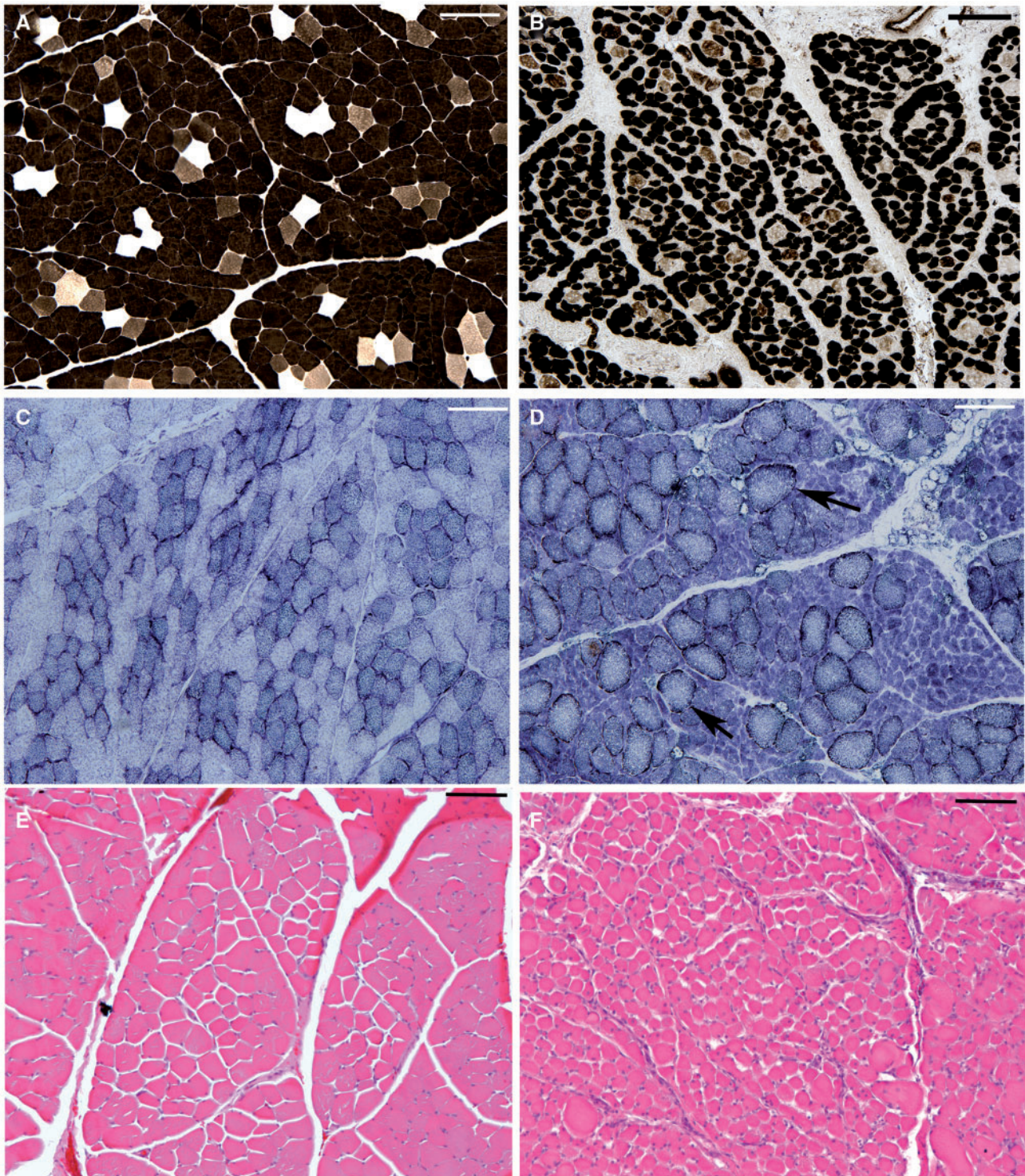


**FIGURE 9.** Representative images showing profound fiber atrophy in the biceps muscle ipsilateral to the lesion following avulsion with myelotomy, (**B, D, F**) compared to the normal fiber diameters of the contralateral biceps (**A, C, E**), as demonstrated by adenosine triphosphatase (ATPase) staining (**A, B**), nicotinamide adenine dinucleotide hydrogen-tetrazolium reductase (NADH-TR) staining (pH 9.4) (**C, D**), and hematoxylin and eosin (H&E) (**E, F**). Specifically the right biceps displayed fibers that were of small diameter and frequently had angulated profiles. Note that NADH-TR staining revealed numerous fibers with zones of central pallor surrounded by an outer zone of relatively darker staining typical of targetoid fibers (**D**). All scale bars: 100  $\mu$ m.

may reflect axon trajectories not disrupted by the avulsion and/or myelotomy, differential support of individual motor neurons, or simply a more delayed degeneration process for some neurons. While it is currently unclear how survival of motor neurons at the level of nerve root avulsion affects recovery, future studies with this experimental model could explore potential mechanisms.

Interestingly, the limited degree of motor neuron death following avulsion injury in our large animal model of neonatal BPI is markedly dissimilar to the near-complete loss observed in adult small animal models of brachial plexus injury (9, 56–60). While we used similar techniques to create avulsion only injury, we observed only a 25% to 33% cell loss across injury levels at 6 weeks. Even in the setting of avulsion and myelotomy, only approximately half of the spinal motor neurons at the levels of injury underwent cell death (range: 45%–66%). This overt difference in the models may reflect species-specific responses, age effects, or both. For the former, small animals have a relatively short distance from the nerve root to the motor neuron. Therefore, the more proximal site of axon transection in rodent models may be far more injurious to motor neurons than the same injury in the piglet. Notably, the size of the piglet nerve roots and spinal cord are relatively similar to those of a human infant, so the preservation of some motor neurons in the swine model suggests that the same may be true for human infant nerve root avulsion.

In addition to anatomic size, the age at which nerve root avulsion occurs may have a dramatic effect on motor neuron survival. In particular, “younger” motor neurons may be primed for more robust survival, especially in the postnatal period. Notably, the profile of trophic support for neurons is known to vary greatly through the course of development and could influence the response to injury (61–63). While this may reflect an evolutionary strategy to reverse major nervous system injury due to birth trauma (64), further studies are needed to characterize the age-dependent survival capacity of spinal motor neurons after axotomy. Regardless, in cases of neonatal brachial plexus injury without complete avulsion resulting in disconnection of the nerve root, survival of the motor neurons is essential to enable motor fiber regeneration all the way down the limb of an infant, which is not thought possible in the adult.

Neuropathological examination also demonstrated the surprisingly dynamic and progressive nature of neonatal BPI. Similar to previous observations in clinical cases and animal models of severe brain and spinal cord injury (45, 65–68), we found that white matter continued to degenerate even many weeks after the initiating injury, as evidenced by ongoing axonal transport interruption demonstrated by accumulation of APP. Similarly, ultrastructural changes to axons were demonstrated subacutely following a model of avulsion in cats (69). As such, it appears that the initial mechanical injury triggered a persistent, progressive degenerative process, particularly of white matter axons, as has recently been observed in traumatic brain injury (45). This was accompanied by a loss of myelin, likely secondary to axonal loss and dysfunction. Interestingly, previous studies in brain and spinal cord injury indicate that downregulation of myelin protein

genes (70), and apoptosis of oligodendrocytes (71) can occur postinjury and may contribute to progressive white matter degeneration.

As suggested for other CNS injuries, persistent inflammatory changes may also play a contributory role in progressive pathology (45, 72, 73). Here, we observed abundant astrocytosis and microglial reactivity in the spinal cord at 6 weeks postinjury. It is possible these cells contribute to the repair process by clearing debris and absorbing deleterious neurochemicals. In particular, phagocytosis and proteolysis of degenerating axon and myelin fragments would be important to limit inhibitors of short distance axon regeneration and for general tissue recovery (74–76). Notably, Iba-1-positive cells with an amoeboid morphology, consistent with appearance of macrophages, were frequently observed in regions of extensive and active white matter degeneration. Whether this persistent inflammation is responsible for ongoing axonal degeneration or, in contrast, is induced in response to axonal pathology, is unclear. Conspicuously, increased inflammation and gliosis were also observed even on the side of the cord contralateral to lesion, primarily in those animals with avulsion and myelotomy. Notably, although the number of animals was limited, there was some evidence indicating a possible decrease in motor neurons in the contralateral C6 spinal level following avulsion with myelotomy. Given the observation of worse functional deficits contralateral to the lesion in this group, it raises the possibility that persistent and more diffuse neuroinflammatory responses may contribute to cell injury and clinical effects. As such, this model permits the ability to observe the temporal course of both the possible reparative and destructive inflammatory responses and inform potential therapeutic strategies for neonatal BPI.

As anticipated, spinal cord avulsion with and without myelotomy resulted in marked neurogenic muscle atrophy. Notably, fiber-typing studies indicated a degree of preferential type II fiber atrophy, in contrast to the reported mixed fiber atrophy typical of neurogenic atrophy in humans. This may be related to the baseline differences in muscle fiber type pattern and distribution in swine, which have previously been shown to vary with multiple factors including age and strain (77–79). Furthermore, some reports indicate regions with a baseline predominance of type II fibers, consistent with what we observed (77). Thus, the observed differential atrophic fiber type response may be a swine-specific phenomenon.

Taken together, the present data demonstrate potential neuropathological features of nerve root avulsion injury that account for poor functional outcomes. In particular, direct damage to the white matter due to trauma not only appears to affect long tracts traveling through the avulsion site, but also induces greater motor neuron death, progressive axon degeneration and myelin loss, and persistent inflammatory changes. Notably, given the complexity of large animal studies, the number of animals included in this study is small and future experiments may require further validation using a larger sample size for both groups. Nonetheless, in marked contrast to small animal models, even with the most severe neonatal BPI in the piglet some motor neurons survived. Importantly, if this

is also the case for neonatal BPI in humans, there may be rationale to repair the avulsion to permit regeneration of motor axons. Even without considerations of repair, further work is needed to develop strategies that will mitigate progressive neuropathological changes in the spinal cord after neonatal BPI to improve functional outcome.

## REFERENCES

- Foad SL, Mehlman CT, Ying J. The epidemiology of neonatal brachial plexus palsy in the United States. *J Bone Joint Surg* 2008;90:1258–64
- Greenwald AG, Schute PC, Shiveley JL. Brachial plexus birth palsy: A 10-year report on the incidence and prognosis. *J Ped Orthopedics* 1984;4:689–92
- Levine MG, Holroyde J, Woods JR, Jr., et al. Birth trauma: Incidence and predisposing factors. *Obstet Gynecol* 1984;63:792–5
- Pondaag W, Malessy MJ, van Dijk JG, et al. Natural history of obstetric brachial plexus palsy: A systematic review. *Dev Med Child Neurol* 2004;46:138–44
- Lagerkvist AL, Johansson U, Johansson A, et al. Obstetric brachial plexus palsy: A prospective, population-based study of incidence, recovery, and residual impairment at 18 months of age. *Dev Med Child Neurol* 2010;52:529–34
- Narakas AO. [Injuries of the brachial plexus and neighboring peripheral nerves in vertebral fractures and other trauma of the cervical spine]. *Der Orthopade* 1987;16:81–6
- Carlstedt TP. Spinal nerve root injuries in brachial plexus lesions: Basic science and clinical application of new surgical strategies. A review. *Microsurgery* 1995;16:13–6
- van Dijk JG, Pondaag W, Malessy MJ. Obstetric lesions of the brachial plexus. *Muscle Nerve* 2001;24:1451–61
- Koliatsos VE, Price WL, Pardo CA, et al. Ventral root avulsion: An experimental model of death of adult motor neurons. *J Comp Neurol* 1994;342:35–44
- Nordin L, Sinisi M. Brachial plexus-avulsion causing Brown-Sequard syndrome: A report of three cases. *J Bone Joint Surg Br* 2009;91:88–90
- Tavakkolizadeh A, Saifuddin A, Birch R. Imaging of adult brachial plexus traction injuries. *J Hand Surg Br* 2001;26:183–91
- Rhee PC, Pirola E, Hebert-Blouin MN, et al. Concomitant traumatic spinal cord and brachial plexus injuries in adult patients. *J Bone Joint Surg Am* 2011;93:2271–7
- Yoshikawa T, Hayashi N, Yamamoto S, et al. Brachial plexus injury: clinical manifestations, conventional imaging findings, and the latest imaging techniques. *Radiographics: A review publication of the Radiological Society of North America, Inc* 2006;26 Suppl 1:S133–43
- Volle E, Assheuer J, Hedde JP, et al. Radicular avulsion resulting from spinal injury: assessment of diagnostic modalities. *Neuroradiology* 1992;34:235–40
- Hems TE, Birch R, Carlstedt T. The role of magnetic resonance imaging in the management of traction injuries to the adult brachial plexus. *J Hand Surg Br* 1999;24:550–5
- Somashekar D, Yang LJ, Ibrahim M, et al. High-resolution MRI evaluation of neonatal brachial plexus palsy: A promising alternative to traditional CT myelography. *AJNR Am J Neuroradiol* 2014;35:1209–13
- Wu W, Li L. Inhibition of nitric oxide synthase reduces motoneuron death due to spinal root avulsion. *Neurosci Lett* 1993;153:121–4
- Bertelli JA, Mira JC. Brachial plexus repair by peripheral nerve grafts directly into the spinal cord in rats. Behavioral and anatomical evidence of functional recovery. *J Neurosurg* 1994;81:107–14
- Bertelli JA, Orsal D, Mira JC. Median nerve neurotization by peripheral nerve grafts directly implanted into the spinal cord: anatomical, behavioural and electrophysiological evidences of sensorimotor recovery. *Brain Res* 1994;644:150–9
- Griffiths IR. Avulsion of the brachial plexus—1. Neuropathology of the spinal cord and peripheral nerves. *J Small Anim Pract* 1974;15:165–76
- Hoffmann CF, Thomeer RT, Marani E. Reimplantation of ventral rootlets into the cervical spinal cord after their avulsion: an anterior surgical approach. *Clin Neurol Neurosurg* 1993;95 Suppl:S112–8
- Carlstedt TP, Hallin RG, Hedstrom KG, et al. Functional recovery in primates with brachial plexus injury after spinal cord implantation of avulsed ventral roots. *J Neurol, Neurosurg Psychiatry* 1993;56:649–54
- Cao X, Li J, Cao Y, et al. C3,4 transfer for neurotization of C5,6 nerve roots in brachial plexus injury in a rabbit model. *J Reconstr Microsurg* 2003;19:265–70
- Gu YD, Ma MK. Nerve transfer for treatment of root avulsion of the brachial plexus: Experimental studies in a rat model. *J Reconstr Microsurg* 1991;7:15–22
- Inciong JG, Marrocco WC, Terzis JK. Efficacy of intervention strategies in a brachial plexus global avulsion model in the rat. *Plast Reconstr Surg* 2000;105:2059–71
- Liu LJ, Zhu JK, Xiao JD. [Rescue of motoneuron from brachial plexus nerve root avulsion induced cell death by Schwann cell derived neurotrophic factor]. *Zhongguo Xiu Fu Chong Jian Wai Ke Za Zhi* 1999;13:295–8
- Moissonnier P, Duchossoy Y, Lavielle S, et al. Lateral approach of the dog brachial plexus for ventral root reimplantation. *Spinal Cord* 1998;36:391–8
- Roldan P, Broseta J, Gonzalez-Darder J, et al. [Central pain model after brachial plexus avulsion. Experimental study in rats]. *Arch Neurobiol (Madr)* 1982;45:225–36
- Spinner RJ, Khoobehi A, Kazmi S, et al. Model for avulsion injury in the rat brachial plexus using passive acceleration. *Microsurgery* 2000;20:94–7
- Haninec P, Dubovy P, Samal F, et al. Reinnervation of the rat musculocutaneous nerve stump after its direct reconnection with the C5 spinal cord segment by the nerve graft following avulsion of the ventral spinal roots: A comparison of intrathecal administration of brain-derived neurotrophic factor and Cerebrolysin. *Exp Brain Res* 2004;159:425–32
- Muneton-Gomez V, Taylor JS, Averill S, et al. Degeneration of primary afferent terminals following brachial plexus extensive avulsion injury in rats. *Biomedica* 2004;24:183–93
- Rodrigues-Filho R, Campos MM, Ferreira J, et al. Pharmacological characterisation of the rat brachial plexus avulsion model of neuropathic pain. *Brain Res* 2004;1018:159–70
- Zhang CG, Welin D, Novikov L, et al. Motoneuron protection by N-acetyl-cysteine after ventral root avulsion and ventral rhizotomy. *Br J Plast Surg* 2005;58:765–73
- Del Fabbro L, Borges Filho C, et al. Effects of Se-phenyl thiazolidine-4-carboselenoate on mechanical and thermal hyperalgesia in brachial plexus avulsion in mice: mediation by cannabinoid CB1 and CB2 receptors. *Brain Res* 2012;1475:31–6
- Wang B, Chen L, Liu B, et al. Differentiation of endogenous neural stem cells in adult versus neonatal rats after brachial plexus root avulsion injury. *Neural Regen Res* 2012;7:1786–90
- Zhao XC, Wang LL, Wang YQ, et al. Activation of phospholipase-C $\gamma$  and protein kinase C signal pathways helps the survival of spinal motoneurons injured by root avulsion. *J Neurochem* 2012;121:362–72
- Li K, Cao RJ, Zhu XJ, et al. Erythropoietin attenuates the apoptosis of adult neurons after brachial plexus root avulsion by downregulating JNK phosphorylation and c-Jun expression and inhibiting c-PARP cleavage. *J Mol Neurosci* 2015;56:917–25
- Wang L, Yuzhou L, Yingjie Z, et al. A new rat model of neuropathic pain: Complete brachial plexus avulsion. *Neurosci Lett* 2015;589:52–6
- Ochiai H, Ikeda T, Mishima K, et al. Development of a novel experimental rat model for neonatal pre-ganglionic upper brachial plexus injury. *J Neurosci Methods* 2002;119:51–7
- Tada K, Ohshita S, Yonenobu K, et al. Experimental study of spinal nerve repair after plexus brachialis injury in newborn rats: a horseradish peroxidase study. *Exp Neurol* 1979;65:301–14
- Wu Y, Li Y, Liu H, Wu W. Induction of nitric oxide synthase and motoneuron death in newborn and early postnatal rats following spinal root avulsion. *Neurosci Lett* 1995;194:109–12
- Birch RBG, Wynn Parry CB. *Surgical disorders of the peripheral nerves*. Edinburgh: Churchill Livingstone 1998
- Smith DH, Chen XH, Nonaka M, et al. Accumulation of amyloid beta and tau and the formation of neurofilament inclusions following diffuse brain injury in the pig. *J Neuropathol Exp Neurol* 1999;58:982–92
- Gentleman SM, Nash MJ, Sweeting CJ, Graham DI, Roberts GW. Beta-amyloid precursor protein (beta APP) as a marker for axonal injury after head injury. *Neurosci Lett* 1993;160:139–44
- Johnson VE, Stewart JE, Begbie FD, et al. Inflammation and white matter degeneration persist for years after a single traumatic brain injury. *Brain* 2013;136:28–42

46. Sherriff FE, Bridges LR, Sivaloganathan S. Early detection of axonal injury after human head trauma using immunocytochemistry for beta-amyloid precursor protein. *Acta Neuropathol (Berl)* 1994;87:55–62
47. Oo TF, Siman R, Burke RE. Distinct nuclear and cytoplasmic localization of caspase cleavage products in two models of induced apoptotic death in dopamine neurons of the substantia nigra. *Exp Neurol* 2002;175:1–9
48. Bakshi A, Keck CA, Koshkin VS, et al. Caspase-mediated cell death predominates following engraftment of neural progenitor cells into traumatically injured rat brain. *Brain Res* 2005;1065:8–19
49. Chen Z, Kontonotas D, Friedmann D, et al. Developmental status of neurons selectively vulnerable to rapidly triggered post-ischemic caspase activation. *Neurosci Lett* 2005;376:166–70
50. Guth L, Samaha FJ. Procedure for the histochemical demonstration of acetylmiosin ATPase. *Exp Neurol* 1970;28:365–7
51. Dubowitz V, Sewry C, Oldfors A. *Muscle Biopsy: A Practical Approach*. 4th Edition edition. Philadelphia, Saunders Elsevier 2013
52. Chen LJ, Zhang FG, Li J, et al. Expression of calcitonin gene-related peptide in anterior and posterior horns of the spinal cord after brachial plexus injury. *J Clin Neurosci* 2010;17:87–91
53. Piehl F, Arvidsson U, Johnson H, et al. GAP-43, aFGF, CCK and alpha-and beta-CGRP in rat spinal motoneurons subjected to axotomy and/or dorsal root severance. *Eur J Neurosci* 1993;5:1321–33
54. Johnson VE, Stewart W, Smith DH. Axonal pathology in traumatic brain injury. *Exp Neurol* 2013;246:35–43
55. Gu Y, Spasic Z, Wu W. The effects of remaining axons on motoneuron survival and NOS expression following axotomy in the adult rat. *Dev Neurosci* 1997;19:255–9
56. Li L, Wu W, Lin LF, et al. Rescue of adult mouse motoneurons from injury-induced cell death by glial cell line-derived neurotrophic factor. *Proc Natl Acad Sci USA* 1995;92:9771–5
57. Penas C, Casas C, Robert I, et al. Cytoskeletal and activity-related changes in spinal motoneurons after root avulsion. *J Neurotrauma* 2009;26:763–79
58. Wu W. Expression of nitric-oxide synthase (NOS) in injured CNS neurons as shown by NADPH diaphorase histochemistry. *Exp Neurol* 1993;120:153–9
59. Kishino A, Ishige Y, Tatsuno T, et al. BDNF prevents and reverses adult rat motor neuron degeneration and induces axonal outgrowth. *Exp Neurol* 1997;144:273–86
60. Piehl F, Hammarberg H, Tabar G, et al. Changes in the mRNA expression pattern, with special reference to calcitonin gene-related peptide, after axonal injuries in rat motoneurons depends on age and type of injury. *Exp Brain Res* 1998;119:191–204
61. Maisonpierre PC, Belluscio L, Friedman B, et al. NT-3, BDNF, and NGF in the developing rat nervous system: Parallel as well as reciprocal patterns of expression. *Neuron* 1990;5:501–9
62. Maisonpierre PC, Belluscio L, Squinto S, et al. Neurotrophin-3: A neurotrophic factor related to NGF and BDNF. *Science* 1990;247:1446–51
63. Koliatsos VE, Clatterbuck RE, Winslow JW, et al. Evidence that brain-derived neurotrophic factor is a trophic factor for motor neurons in vivo. *Neuron* 1993;10:359–67
64. Weil ZM, Norman GJ, DeVries AC, et al. The injured nervous system: A Darwinian perspective. *Prog Neurobiol* 2008;86:48–59
65. Ek CJ, Habgood MD, Dennis R, et al. Pathological changes in the white matter after spinal contusion injury in the rat. *PLoS One* 2012;7:e43484
66. Chen XH, Siman R, Iwata A, et al. Long-term accumulation of amyloid-beta, beta-secretase, presenilin-1, and caspase-3 in damaged axons following brain trauma. *Am J Pathol* 2004;165:357–71
67. Chen XH, Johnson VE, Uryu K, et al. A lack of amyloid beta plaques despite persistent accumulation of amyloid beta in axons of long-term survivors of traumatic brain injury. *Brain Pathol* 2009;19:214–23
68. Crowe MJ, Bresnahan JC, Shuman SL, et al. Apoptosis and delayed degeneration after spinal cord injury in rats and monkeys. *Nat Med* 1997;3:73–6
69. Hoffmann CF, Choufoer H, Marani E, et al. Ultrastructural study on avulsion effects of the cat cervical moto-axonal pathways in the spinal cord. *Clin Neurol Neurosurg* 1993;95 Suppl:S39–47
70. Wrathall JR, Li W, Hudson LD. Myelin gene expression after experimental contusive spinal cord injury. *J Neurosci* 1998;18:8780–93
71. Shaw K, MacKinnon MA, Raghupathi R, et al. TUNEL-positive staining in white and grey matter after fatal head injury in man. *Clin Neuropathol* 2001;20:106–12
72. Faden AI, Wu J, Stoica BA, et al. Progressive inflammatory-mediated neurodegeneration after traumatic brain or spinal cord injury. *Br J Pharmacol* 2015 [Epub ahead of print]
73. Allison DJ, Ditor DS. Immune dysfunction and chronic inflammation following spinal cord injury. *Spinal Cord* 2015;53:14–8
74. Domeniconi M, Filbin MT. Overcoming inhibitors in myelin to promote axonal regeneration. *J Neurol Sci* 2005;233:43–7
75. McKerracher L, David S, Jackson DL, et al. Identification of myelin-associated glycoprotein as a major myelin-derived inhibitor of neurite growth. *Neuron* 1994;13:805–11
76. Wang L, Hu B, Wong WM, et al. Glial and axonal responses in areas of Wallerian degeneration of the corticospinal and dorsal ascending tracts after spinal cord dorsal funiculotomy. *Neuropathology* 2009;29:230–41
77. Skorjank D, Salehar A, Erzen I, et al. Pattern of fibre type distribution within muscle fascicles of pigs (*Sus scrofa domestica*). *Czech J Anim Sci* 2007;52:103–9
78. Karlsson A, Klont R, Fernandez X. Skeletal muscle fibres as factors for pork quality. *Livestock Production Science* 1999;60:255–69
79. Ryu Y, Choi Y, Lee S, et al. Comparing the histochemical characteristics and meat quality traits of different pig breeds. *Meat Science* 2008;80:363–69